Molecular Crystals and Liquid Crystals Incorporating Nonlinear Optics
Publication details, including instructions for authors and subscription information:
http://www.tandfonline.com/loi/gmcl17

The Low-Q Diffractometer at the Los Alamos Neutron Scattering Center

P. A. Seeger [a] , R. P. Hjelm Jr [a] & M. J. Nutter [a]
[a] Los Alamos National Laboratory, Los Alamos, NM, 87545, USA
Version of record first published: 22 Sep 2006.

To cite this article: P. A. Seeger , R. P. Hjelm Jr & M. J. Nutter (1990): The Low-Q Diffractometer at the Los Alamos Neutron Scattering Center, Molecular Crystals and Liquid Crystals Incorporating Nonlinear Optics, 180:1, 101-117

To link to this article: http://dx.doi.org/10.1080/00268949008025793

Mol. Cryst. Liq. Cryst., 1990, Vol. 180A, pp. 101–117
Reprints available directly from the publisher
Photocopying permitted by license only

Printed in the United States of America

The Low-Q Diffractometer at the Los Alamos Neutron Scattering Center

P. A. SEEGER, R. P. HJELM, JR. and M. J. NUTTER
Los Alamos National Laboratory, Los Alamos, NM 87545, USA

The Low-Q Diffractometer at the Los Alamos Neutron Scattering Center is now operational, and a variety of calibration experiments have been performed. A description of the instrument is presented, emphasizing its special and unique features. In particular, the "dynamic gravity focusing" device has been demonstrated to extend the useful wavelength range to values which would otherwise fall below the beam stop onto the detector. The downstream monitor in the beam stop has also been demonstrated, allowing data reduction even from strongly scattering samples without the necessity of a separate transmission measurement. Examples of data as displayed to users during data acquisition from various experiments shown. Procedures to combine data from a wide wavelength range into Q space are discussed, and three examples are shown which illustrate the dynamic range of the instrument.

1. INTRODUCTION

The Low-Q Diffractometer (LQD) at the Los Alamos Neutron Scattering Center (LANSCE) is now operational. Calibration measurements have been performed, with results in excellent agreement with expectations. Some initial experiments have been carried out in collaboration with experienced users; these results are also very promising.

The LQD, which has been described in the proceedings of the last two meetings of the International Collaboration on Advanced Neutron Sources,[1,2] was designed to provide scientists in the United States with an instrument comparable to (and in some ways complementary to) the best reactor-based small-angle scattering instruments. Using the broad wavelength range of neutrons from a pulsed source, the LQD is most advantageous for experiments requiring measurement over an extended range of momentum transfer (Q) because its full Q range (0.003 to 0.5 $Å^{-1}$) is recorded without changing configuration or moving the detector. A prototype instrument was operated in December, 1985, using the liquid hydrogen moderator and a prototype Anger camera. First tests of the almost completed instrument were made in September, 1986, using a two-dimensional ^3He proportional counter. Final testing was conducted during the most recent accelerator cycle (September through November, 1987), and an experimental program was initiated. This report gives a brief description of the instrument, with emphasis on the special

and/or unique features of the LQD: converging collimation, dynamic gravity focusing, the visual alignment system, and the downstream monitor. Some of the data collected (and its bearing on instrument performance) is discussed.

2. INSTRUMENT DESCRIPTION

An elevation view of the instrument is shown in Figure 1, and the specifications (as it is expected to be configured in 1988) are given in Table I. The liquid hydrogen moderator produces a neutron spectrum which peaks at about 2.4 Å but has usable flux from 0.3 to 20 Å. A low-pass filter of single-crystal MgO will be installed in 1988 to attenuate the short wavelength part of the spectrum in order to reduce background and inelastic scattering. The resulting spectral range will be that of most interest for small-angle scattering. The filter will be removable for experiments requiring short wavelengths.

Collimation is of the "pinhole" type, with two circular apertures 3.76 m apart. The collimation system has been optimized using Monte Carlo, analytic, and ray-tracing techniques.[3] The optimization condition is simply that aperture sizes should converge to a point at the detector,[4] as indicated by the shading in Figure 1. Multiple entrance and exit apertures may be used, provided that beam scrapers are also installed to prevent neutrons entering one aperture from crossing over to the wrong exit. The "Primary path" pipe in Figure 1 will eventually contain a rotating assembly to allow three different sets of beam scrapers, probably with one, seven, and nineteen holes, respectively. At present only the single-aperture collimator is completed, and the pipe is nearly filled with shielding material. Multiple aperture sets, all converging to the same point at the detector, will increase the intensity without affecting the resolution.[5]

The detector resolution and efficiency were not considered in the optimization; they are assumed to be good enough not to affect the collimator design. A two-dimensional ^{3}He proportional counter[6] is presently being used, which has a standard deviation of position determination of nearly 4 mm, and rather low efficiency. Plans call for a new Anger camera,[7] which has a resolution better than 1.5 mm and which will be digitized in bins 2.3 mm square. This will not contribute significantly to the resolution if the sample-to-detector distance is greater than 3 m. Instrument resolution parameters are shown in Table I, expressed as standard deviations (root mean square). To find the resolution (ΔQ) at an intermediate value of momentum transfer Q, multiply the $\Delta Q/Q$ value by Q and then take the square root of the sum of the squares of that number and the ΔQ at small Q. Intensity values in the table assume a proton current of 30 μA, and the single-aperture collimation system. When a multiple-aperture system is used the intensity will be seven times higher, and when LANSCE reaches its design current of 100 μA the intensity will be another factor of three higher. The values given have also been multiplied by detector efficiency.

At the 12 Hz pulse repetition rate presently in use, neutrons recorded at the end of the frame fall 34 mm under the influence of gravity. The "Gravity focusing" device indicated in Figure 1 and described in the next section selects the neutrons

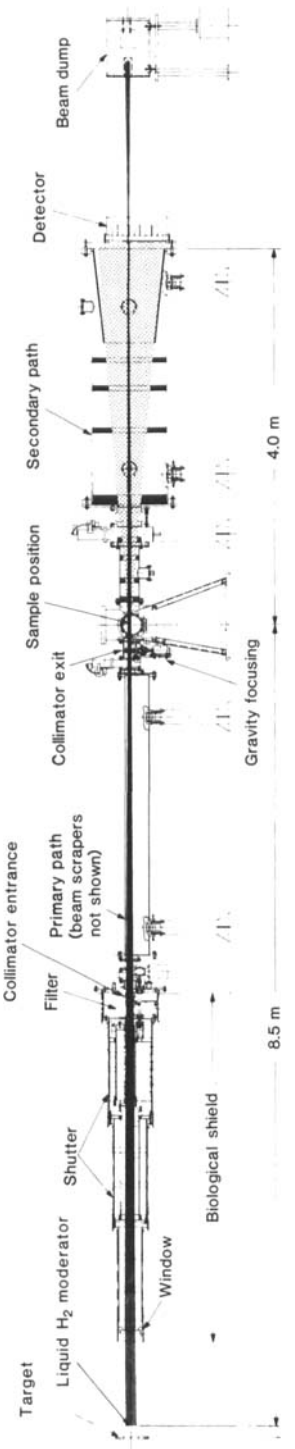

FIGURE 1 Plan view of the Low-Q Diffractometer.

TABLE I

LQD Specifications, 1988

Wavelength range, λ	0.5 - 13 Å
Scattering angle, θ	5 - 75 mrad
Momentum transfer (units of $\hbar$), Q	0.003 - 0.5 $Å^{-1}$
Beam diameter at sample:	
Single-aperture collimator	10 mm
Multiple-aperture collimator	35 mm
Resolution using ^{3}He detector:	
$\Delta\lambda/\lambda$ (rms)	0.009
$\Delta\theta$ (rms)	1.6 mrad
small Q, ΔQ (rms)	0.0013 $Å^{-1}$
large Q, $\Delta Q/Q$ (rms)	0.010
Resolution using Anger camera:	
$\Delta\lambda/\lambda$ (rms)	0.006
$\Delta\theta$ (rms)	1.3 mrad
small Q, ΔQ (rms)	0.0010 $Å^{-1}$
large Q, $\Delta Q/Q$ (rms)	0.007
Intensity at 30 μA with single aperture:	
0.6 to 1.6 Å (32 to 230 meV)	0.6×10^4 n/s
1.6 to 5.0 Å (3.3 to 32 meV)	2.4×10^4 n/s
5.0 to 17 Å (0.3 to 3.3 meV)	0.7×10^4 n/s

Staff

Philip A. Seeger, instrument responsible
Jill Trewhella, biological program
Rex P. Hjelm, Jr., biology/polymers
Art Williams, metallurgy
A. C. Lawson, metallurgy
Murlin J. Nutter, detectors and electronics
Rod Hardy, mechanical technician

Any of the above may be reached at the following address:

LANSCE, MS/H805
Los Alamos National Laboratory
P. O. Box 1663
Los Alamos, NM 87545
(505)667-6069, or FTS 843-6069

which have parabolic trajectories that strike the detector at its center; otherwise the size of the beam stop would have to be increased and software corrections made to the data.

The sample position of the LQD is designed to allow versatility of environments. Up to 1 m of pipe can be removed for large apparatus. The principal sample chamber is an evacuated vertical cylinder 30 cm in diameter and 46 cm tall, with the beam elevation 18 cm above the bottom. Valves are positioned to isolate the chamber for changing samples and apparatus. The chamber has access flanges on the top, bottom, and both sides. The bottom flange is reserved for installation of a displex refrigerator; we expect user-supplied apparatus generally to be mounted through the top of the chamber. Detailed dimensions will be supplied on request.

For experiments requiring rapid sample changing capability and/or which can not be run in vacuum, there is an "air chamber" insert with fused silica windows which can be mounted in one of the side ports to the sample chamber. This has a rectangular cross section, 155 mm tall by 80 mm in the beam direction, and the beam centerline is 105 mm above its floor. We have a four-position sample changer (modified from a Gilford spectrophotometer) which can be mounted in this air insert and which provides temperature control by circulating refrigerated or heated liquid. Standard 1-cm-wide fused silica spectrophotometer cells are used, with pathlengths between 1 and 10 mm; optimal pathlength depends on the neutron transmission of the sample, which is generally determined by its hydrogen content. A mask on the changer limits the neutron beam to about 9 mm diameter to prevent reflections from the edges of the cells. A more versatile changer is under design.

A significant advantage of the converging collimation system is that the detector position is fixed, and thus it is practical to install shielding baffles in the secondary pipe; these are made of polyethelyne loaded with B_4C, with tapered apertures so that no surfaces can be seen both from the detector and from the sample. Because of detector sensitivity to gamma rays, the only neutron capturing material which should be allowed in the direct beam or within 1 m of the detector is ^6Li; in particular, no Cd should ever be allowed in the vicinity of the instrument. The cone shown just before the detector will be made of pressed ^6LiF.

The detector represented in Figure 1 is an Anger camera. Its 50-mm-thick optical glass disperser plate is used as the vacuum window, so that there are no windows (other than an Al foil light shield and reflector) in front of the scintillator. The detector area (280 mm × 432 mm) is off-center to increase the range of momentum transfer. Using our optimized encoding scheme,[4] the time per event has been reduced (from the value of several μs in the standard Anger camera) to only 0.4 μs. This is very significant because of the high instantaneous data rates expected at LANSCE. The Anger camer is still under development. As an alternative detector until the Anger camera is ready, a ^3He position-sensitive proportional counter purchased from the Risø National Laboratory in Denmark[6] is being used. A comparison between this detector and the downstream monitor (which is a glass scintillator of the same type as used in the Anger camera) is presented in a later section.

Another unique feature of the LQD is the visual alignment system. An optical mirror at an angle of 45° may be lowered into the beam path at a position 1 m in

front of the detector, and a telescope is permanently attached at a viewport on the side of the secondary pipe. This allows a check of the collimator and sample alignment. The mirror may also be rotated by 90° to give a view of the beamstop. This is important because the beamstop must be precisely oriented so that the opening into the monitor detector is aligned with the instrument axis.

3. GRAVITY FOCUSER

By moving the collimator exit aperture upward at the correct constant acceleration starting from rest each time a proton pulse hits the target, the trajectory for each neutron wavelength (velocity) may be selected such that all intersect at the center of the detector. The acceleration depends on the ratio of flight paths[1]; for the LQD it is 0.239 g, or 2.30 m/s^2. The duration of the motion is just long enough for the frame-overlap neutrons (i.e., neutrons which will reach the detector at the same time that the next proton pulse is hitting the target) to reach the collimator exit, or 40 ms in the present configuration at 12 Hz repetition rate. This leaves 21 ms to reinitialize between pulses. The maximum upward displacement is $\frac{1}{2}$ at^2 = 1.8 mm, which is 22% of the diameter of the aperture. The load to be moved is a disk of Pb and ^{6}LiF, 2.5 cm thick and 10 cm in diameter, with a mass of approximately 2.3 kg. The disk is in vacuum, and the actuating shaft penetration is sealed with a welded bellows.

To achieve a high degree of reliability, the system was implemented with simple, commercially available components. The requirements are not exotic; the most difficult is the recycle time, which demands a relatively large restoring force. The prime mover is a hydraulic servoactuator system from Moog, Inc., model 853-A72319-1, with a 7 cm^2 cylinder and 2.5 cm stroke, driven by a 20 l/minute servo

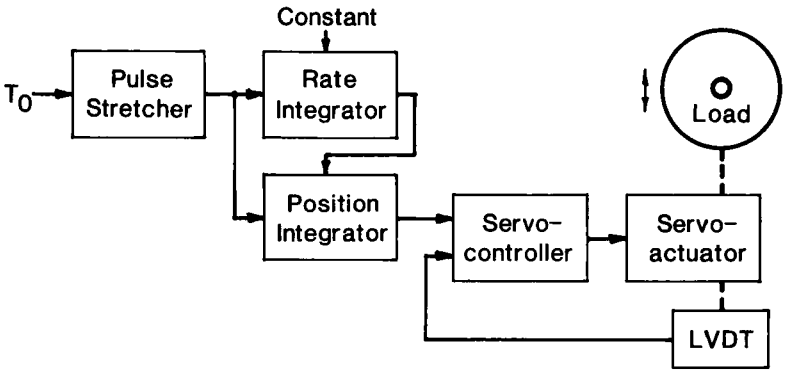

FIGURE 2 Block diagram of the LQD gravity focusing system. By double integrating a constant voltage for a time interval determined by the pulse stretcher, the desired quadratic signal is generated. This is compared to a feedback signal from a position encoder (LVDT, linear variable differential transformer) on the actuator shaft, and the correction signal is applied to the hydraulic servoactuator to move the aperture plate in the desired pattern.

valve. The functions indicated in the block diagram in Figure 2 are also implemented using standard modules from Moog, Inc. They provide the signal conditioning to convert the "Time Zero" signal (i.e., protons on target) into the prescribed constant acceleration motion of the load. The block marked "LVDT" is a linear variable differential transformer for position feedback readout from the actuator shaft.

After a tentative selection of hardware, a simulation of the performance was conducted on an IBM-XT using the program TUTSIM.[8] Physical parameters of mass, area, pressure, bulk modulus, voltage gain, and time constants were entered into various interconnected blocks and the resulting system of differential equations was solved. The simulation indicated that the hardware was capable of moving the load in the prescribed manner. The return-stroke acceleration was predicted to be 40 g; this led us to redesign the attachment of the load to the actuating shaft. Similarly, the electronic modules were simulated with the program MicroCAP II.[9] The various operational amplifiers and their interconnections and feedback elements were simulated to verify the proper operation and generation of the desired signal waveforms. The resulting hardware waveforms (Figure 3) are in excellent agreement with the predictions from TUTSIM and MicroCAP II.

If the gravity focuser is turned off, an intense beam spot appears below the beam stop at late times, as shown in Figure 4. The excess intensity in this spot is approximately 13% of the total beam in the wavelength range from 15 to 19 Å. With the gravity focuser on, the intensity in the same spot is about 4% of the beam, indicating that the parameters of the device have not yet been optimized. All of the necessary adjustments are available, and it will be straight forward to improve the performance of the gravity focuser at the beginning of the next run cycle.

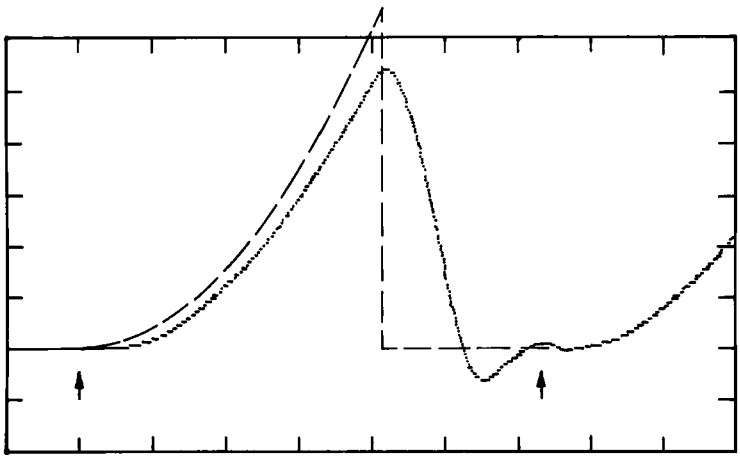

FIGURE 3 Measured waveform from the position transducer on the gravity-focus actuator shaft. The system was triggered twice, at the times indicated by the arrows. The desired quadratic form is superimposed on the digital-oscilloscope output. Sweep speed is 10 ms/division and vertical gain is 62.5 mV/division.

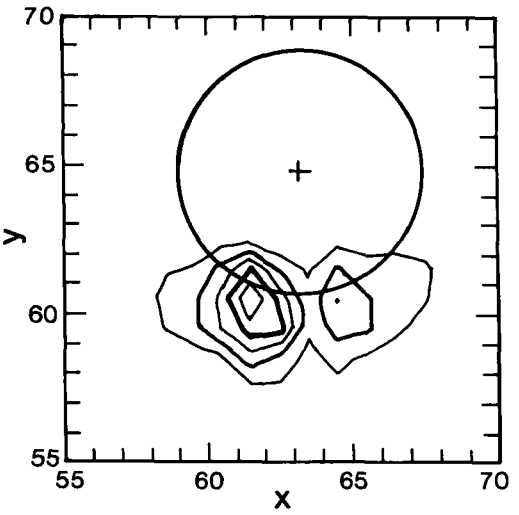

FIGURE 4 Beam intensity appearing below the circular beam stop at late times when the gravity focuser is not operating. The integrated intensity is about 13% of the total beam from 15.7 to 19.0 Å wavelength.

4. DOWNSTREAM MONITOR

The downstream monitor consists of a 2 mm cube of ^{6}Li-loaded scintillator glass centered in the beam stop and exposed to the incident beam through a 1.6-mm diameter hole (see Figure 5). The solid angle subtended by the monitor from the moderator is 0.0126 μster, and the area of moderator seen is 4.6 cm^2. The light produced by neutron captures in the glass is conducted through a 1-mm diameter quartz fiber, through a vacuum interface, to a photomultiplier tube outside the flight path. Standard electronics are used to amplify, discriminate, and provide appropriate pulses to the data acquisition system.

Since the scintillator is enclosed within a beam stop consisting of ^{6}LiF and Pb, the neutron background is low. However a high γ-ray background rate is observed, due to capture of thermalized neutrons from the beam dump behind the detector and the surrounding room walls and shielding materials. The beam dump will be moved further away, and shielding against backgrounds from other sources in the experimental hall will be improved. In particular, no Cd may be allowed near the detector; at present, the ^{3}He detector has an internal Cd sheet which is probably the main source of the γ-ray problem.

The signal is very low at the latest times measured, and the background correction is significant. To determine the background, it is adequate to approximate the signal as a Maxwellian tail. The resulting flux determination is shown in Figure 6. The flux was also determined by placing a Cd mask with a number of small holes (approximately 1% transmission) at the sample position and removing the beam stop from in front of the main detector. The ratio of the two measurements is

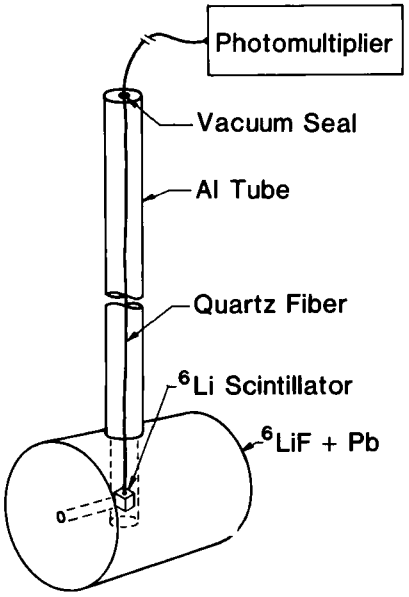

FIGURE 5 Downstream in-beam monitor detector. The aperture is 1.6 mm in diameter, and accepts about 0.8% of the beam. The efficiency of the 2-mm cube of ^{6}Li scintillator glass is 84% at 1 Å.

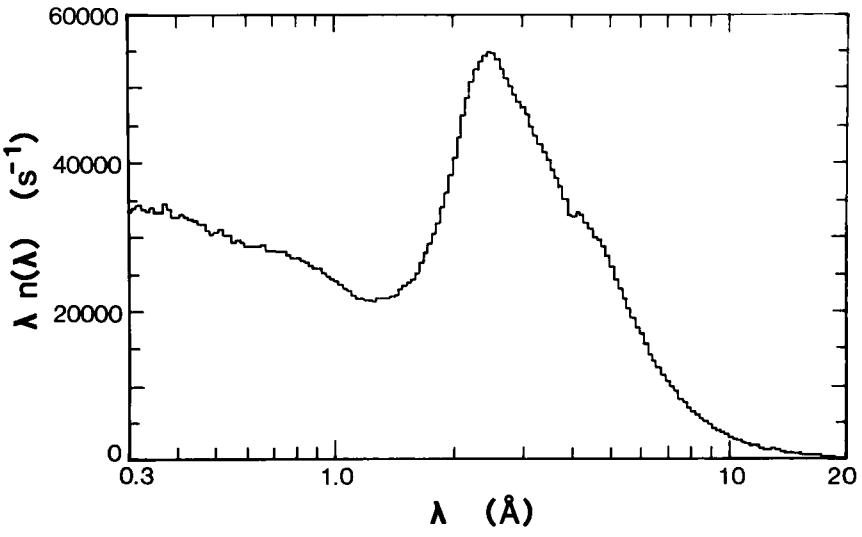

FIGURE 6 Neutron flux from the liquid hydrogen moderator, as measured by the downstream monitor. Data have been corrected for detector efficiency, and normalized to neutrons per Å per second on sample, at a proton current of 30 μA. The peak at 2.4 Å (14 meV) results from the transparency of para-hydrogen to neutrons below that energy. The tail at longer wavelengths is well represented by a Maxwellian which peaks at about 3.4 Å. There is a total thickness of 11 mm of Al windows in the beam, producing Bragg absorption edges and other wavelength-dependent effects.

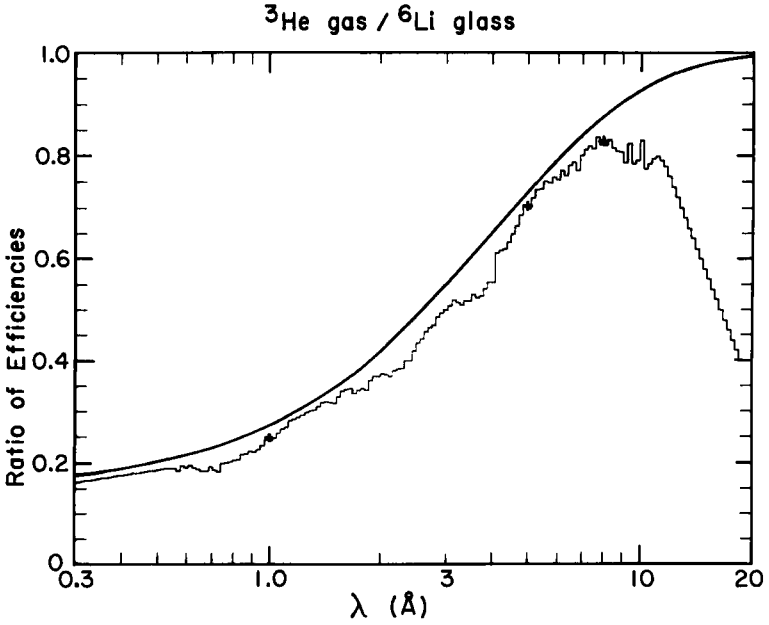

FIGURE 7 Ratio of efficiencies of the ^{3}He gas detector and the ^{6}Li glass scintillator monitor. The measurement has been extrapolated below 0.54 Å, and smoothed above 11 Å. The smooth curve, fitted to the three marked points after adjustment for the absorption of the 9-mm Al window of the gas detector, represents a glass efficiency of 84.5% and a gas efficiency of 23.1% at 1 Å. At the longest wavelengths a large number of neutron capture events appear to be missed in the gas detector, possibly because they occur too close to the front window.

illustrated in Figure 7. The smooth function shows the much lower efficiency of the gas detector compared to the scintillator, and the histogram shows the further defects caused by the thick Al window of the gas detector. To make proper use of short-wavelength neutrons, a scintillator detector (the Anger camera) must be developed.

5. DATA ACQUISITION SYSTEM

The standard LANSCE data acquisition system[10] includes generation of either a linear or logarithmic time-of-flight scale, buffering for neutron events accumulated for each proton pulse, mapping of detector elements, and fast 23-bit histogram memory, all housed in a Fastbus crate and connected to a μVAX-II computer. We record 168 time slices from 963.2 μs to 60880 μs after the proton pulse, with constant $\Delta t/t$ = 2.5%. For each time slice the detector is encoded into a 128 × 128 array, with the angular width of each cell being about 1.0 mrad. One histogram thus includes 2 752 512 words of data, or nearly 8 Mbytes. This memory is readily accomodated in the Fastbus system.

The LANSCE software section has provided programs to control data acquisi-

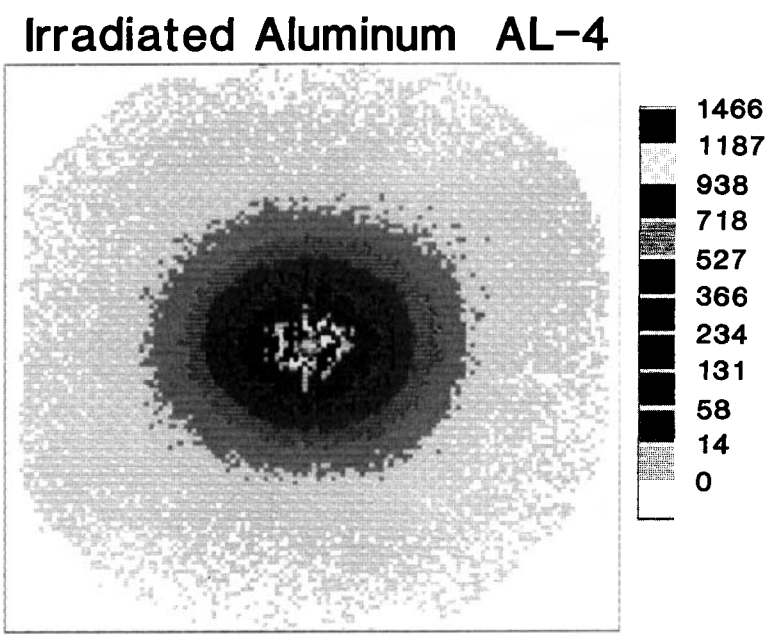

FIGURE 8 Isotropic scattering pattern from voids in a single-crystal Al sample, summed over wavelengths from 9.3 to 13.6 Å. Contrasting colors are used to represent varying histogram levels, which are chosen in a square-root scale.
See Color Plate I.

tion,[11] including one- and two-dimensional graphics for data display on a μVAX workstation. We have also developed graphics to show the two-dimensional detector on an IBM-PC compatible computer (actually an IBM PS/2, model 50) with Enhanced Graphics Adapter (or emulation). Much of the PC-based system uses graphics and communications libraries written (in Turbo PASCAL) by John Hayter at the Oak Ridge National Laboratory. Interactive programs in the μVAX allow data to be accessed, displayed, and analyzed either in real time (while the data are being accumulated) or for archived data. Figures 8–10 illustrate histogram data for the detector area, summed over various wavelength ranges, as displayed on the IBM-PC; note that the color scale has been chosen for high contrast between histogram levels rather than a continuous spectrum. Data may also be mapped into Q-space before display, allowing data from a wide range of wavelengths to be combined without affecting resolution. An example of a block copolymer with a strong peak at a specific Q is given in Figure 11. The data may also be radially averaged and then displayed as plots vs. r or Q.

Additional software is being developed to analyze the test results. These programs will be useful to assess data as it is being collected, or raw data sets which have been archived. After this stage of data *reduction* it should be possible to transport data between various laboratories in a format which will make it practical to share programs for *analysis*. That is, while acquisition and reduction must be specific to each instrument, problems in analysis are common to all users. The

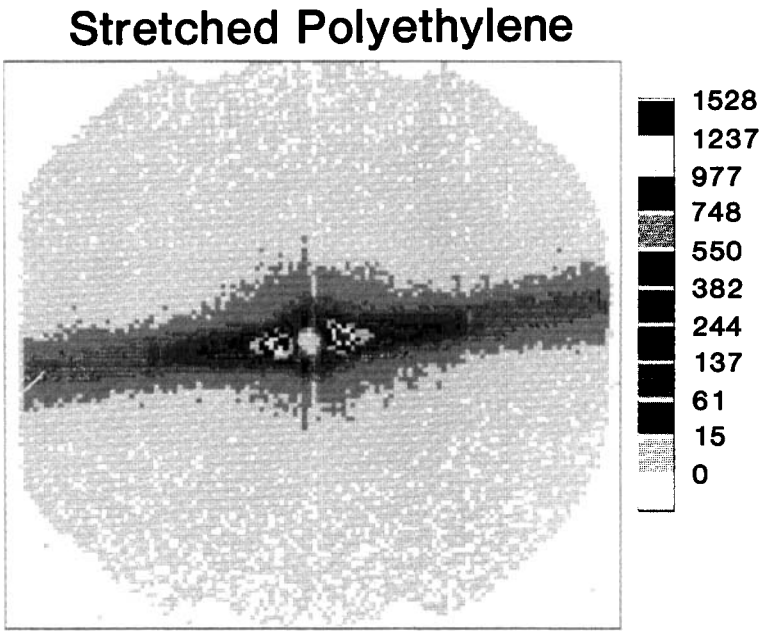

FIGURE 9 Anisotropic scattering pattern from a stretched polyethylene sample. The individual chains in the sample are highly aligned and are much longer than can be observed with small-angle scattering, resulting in measurable scattering only perpendicular to the direction of stretch.
See Color Plate II.

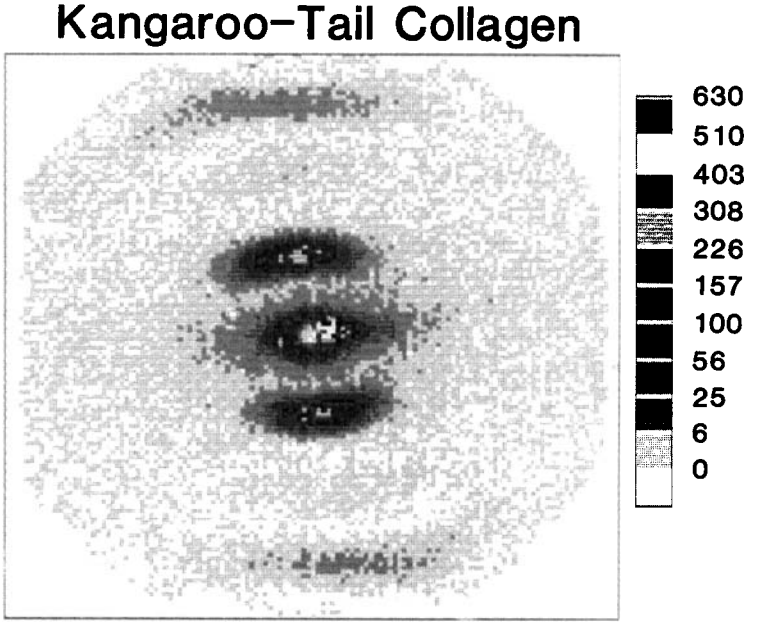

FIGURE 10 Low-resolution diffraction pattern from fibers of kangaroo-tail collagen. In this wavelength range (11.3 to 13.1 Å) the first three orders of the diffraction pattern resulting from the uniform spacing of the individual collagen molecules are visible.
See Color Plate III.

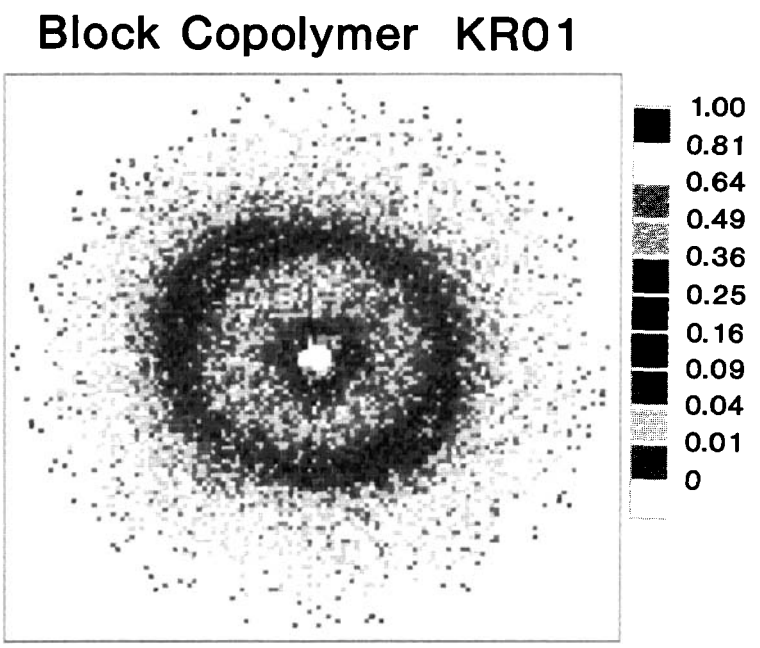

FIGURE 11 Two-dimensional Q map of the scattering from a block copolymer. The data from a larger wavelength range (a factor of 2 in this case) can be combined without spoiling resolution if they are first converted to Q space. This sample appears to have a preferred orientation. This display is available in real time to the LQD experimenter.
See Color Plate IV.

transportable format must include relevant histogram bin boundaries and propagated statistical errors. (If the data are raw counts or simple sums over detector elements, the errors follow Poisson statistics and need not be included explicitly.) Header information included in the file should make it possible to reconstruct all operations which have been performed, and should include numeric values of all instrument parameters used. Because of the large amount of data, the format must be compact, but it is most convenient if it is ASCII characters which can be printed or read anywhere by any computer or person.

6. RESULTS

Several of the samples studied have scattering laws which are strongly peaked at a specific value of Q. These provide sensitive tests of the performance of the instrument in their respective Q domains. The scattering from the first of these, the block copolymer sample "KR01" provided by Dale Schaefer of Sandia Laboratory, is shown as a 2-D Q map in Figure 11. This sample is a sufficiently strong scatterer to determine the scattering angle θ at the peak separately for 104 time slices (wavelengths from 1.5 to 19 Å); the measurement confirms the linearity of the detector. Also, the integrated intensity under the peak should be constant. This gives a much smoother flux determination at wavelengths longer than 10 Å than

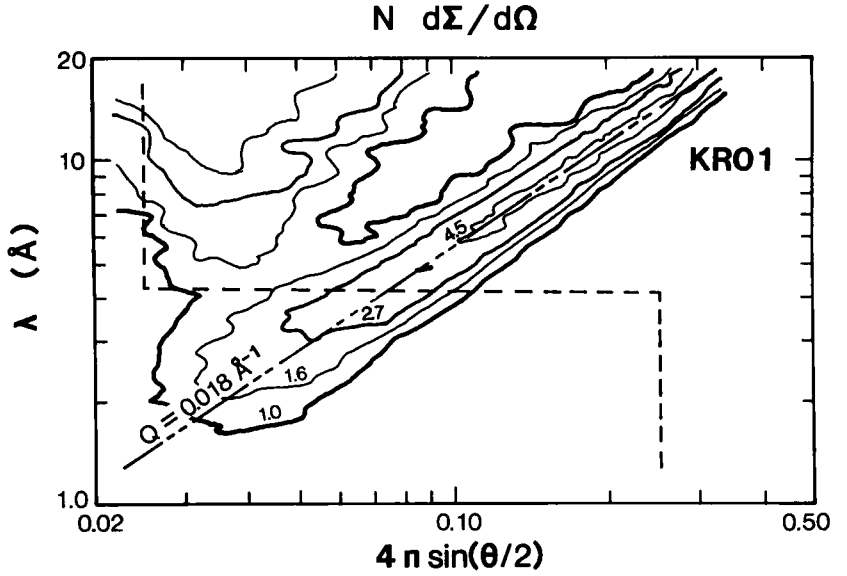

FIGURE 12 The same data as Figure 11, presented as radial averages for each time slice. Radii have been converted to 4π times the sine of half the total scattering angle, and times have been converted to neutron wavelengths; thus Q at any point is the x-coordinate divided by the y-coordinate, and lines of constant Q are diagonals. Background has been subtracted and data have been normalized by the number of transmitted neutrons in each time slice. The dash line separates a region in the lower left which is omitted from further data reduction because the resolution of the detector is not matched to the Q resolution desired.

was obtained from the downstream monitor directly (because of the high gamma background in the scintillator). Figure 12 is a contour plot of the data after radial averaging and background subtraction. Since $Q = [4\pi \sin(\theta/2)]/\lambda$, the value of Q at any point on this map is the ratio of the horizontal and vertical coordinates; lines of constant Q are straight lines parallel to the line shown for $Q = 0.018$ Å^{-1}. Such a plot is a sensitive indicator of instrument performance and of the correctness of data-reduction procedures because the scattering law is a function only of Q and all contours should be constant-Q lines.

The Q-binning scheme[3] joins a linear range from 0.006 Å^{-1} to 0.06 Å^{-1} with logarithmic ranges for smaller and larger Q. Note that the data are accumulated in full-resolution three-dimensional histograms, and the binning may be chosen during data reduction to optimize for intensity or resolution requirements of a particular measurement. Other optimization procedures are under study.[12,13] Each Q bin may contain information derived from many time slices at appropriate radii on the detector; Figure 13 is the statistically weighted average as a function of Q. Data below the dashed line in the lower left of Figure 12 are omitted from the reduced data because the width of the radial zones is more than 1.5 times the width of the relevant Q bin. The units of the ordinate are intended to be absolute; N is scatterers/cm^2 and the differential cross section $d\Sigma/d\Omega$ is in cm^2/ster per scatterer. The absolute scale has not yet been calibrated against the standard samples,[14] however.

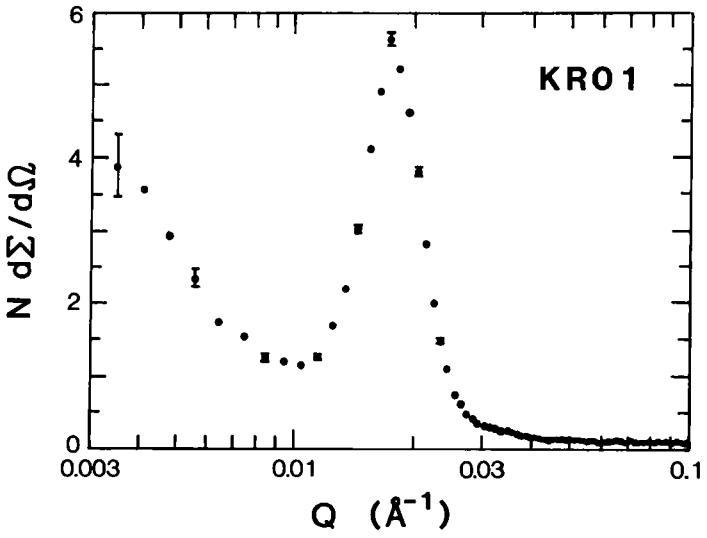

FIGURE 13 The same data as Figures 11 and 12, averaged as a function of Q. The number of neutrons in each Q bin is found by summing the neutrons from those (θ,λ) bins of Figure 12 whose centers fall in the Q bin, and the differential cross section is found by dividing the number of neutrons by the sum ot detector area times number of transmitted neutrons for each included (θ,λ) bin.

To illustrate the lower limit of Q accessible on LQD, a sample of opal (loaned by K. Ibel and A. Wright of the Institute Laue-Langevin[15]) was used. The opal is a face-centered cubic lattice of 2060-Å diameter SiO_2 spheres, with a strong (111) Bragg reflection at $Q = 0.00372$ Å^{-1}. The data in Figure 14 are from a 38-minute run in the standard configuration; 436 692 neutrons were detected in the wavelength

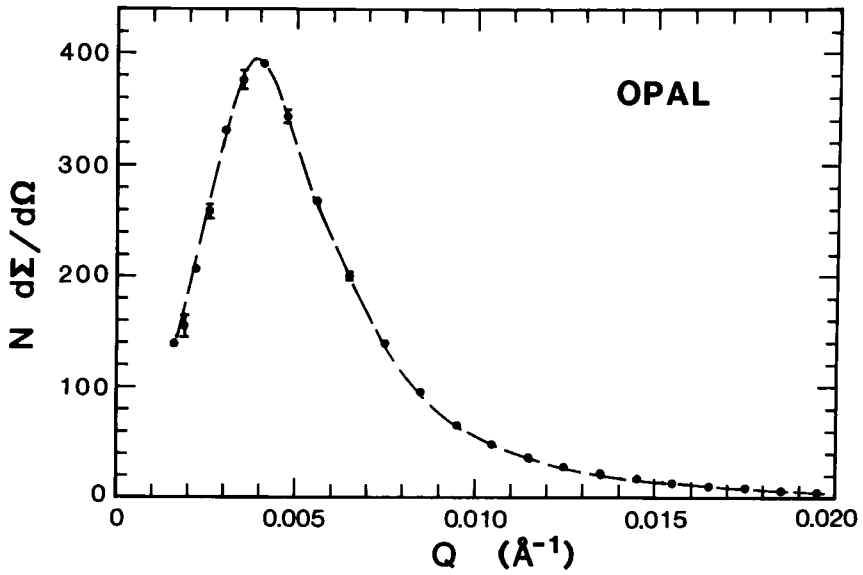

FIGURE 14 Small-angle scattering from a standard opal sample. These data demonstrate the ability of the LQD to measure down to $Q = 0.002$ Å^{-1}. The observed peak is very close to the accepted value of 0.0037 Å^{-1}. A second peak at 0.0061 Å^{-1} is not resolved.

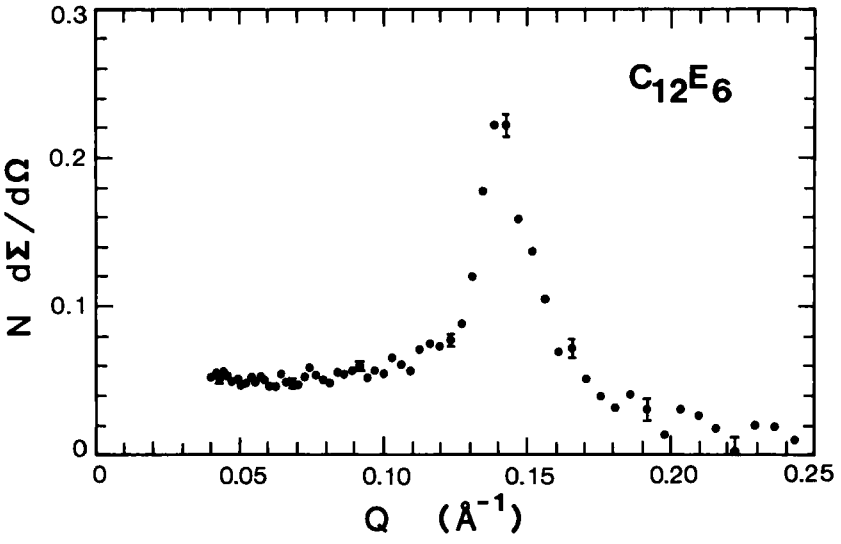

FIGURE 15 Small-angle scattering from a micellar liquid-crystal sample. These data show the current upper limit of the Q range of the LQD; improving shielding of the detector and reducing beam-induced background will extend this range by another factor of two. Note that the examples in Figures 13–15 were all taken with the same instrument configuration.

range from 11 to 19 Å. The curve drawn through the data points peaks at 0.0038 Å^{-1}. A second Bragg reflection at 0.0061 Å^{-1} was not resolved.

An example with a peak at a large value of Q is shown in Figure 15; it is a liquid crystal phase of micelles of *n*-dodecylhexaoxyethylene glycol monoether ($C_{12}E_6$) with a non-ionic surfactant, prepared by Jess Wilcoxon of Sandia Laboratory. The concentration was 65% and the temperature (approximately) 18 C. The phase was presumably cubic. The location of the peak at $Q = 0.14$ Å^{-1} is in good agreement with neutron scattering measurements on a similar sample on the 30-m SANS instrument at the Oak Ridge National Laboratory.

These three examples demonstrate the dynamic range of the LQD. All were taken in the same configuration of the machine; only software parameters of the data reduction were adjusted to optimize for a given Q range.

Note Added in Proof:

The instrument was fully operational and was included in a formal program for outside experimenters in 1988 and 1989. Potential users of the LQD are urged to contact members of our scientific research team as listed in Table I directly.

Acknowledgments

The construction of the LQD is a joint effort of the Life Sciences and Physics Divisions of Los Alamos National Laboratory. We could not have come so far in achieving our goals without the active support and cooperation of colleagues at other neutron-scattering facilities. In particular we would like to thank

the members of our design review committee: J. M. Carpenter (IPNS), J. E. Epperson (IPNS), J. B. Hayter (ORNL), R. Pynn (ILL), K. Rhyne (NBS), J. M. Rowe (NBS), D. Schaefer (Sandia), and J. W. White (Australian Nat. Univ.) This work was performed under the auspices of the United States Department of Energy.

References

1. P. A. Seeger, A. Williams and J. Trewhella, Proceedings of the Eighth Meeting of the International Collaboration on Advanced Neutron Sources, report RAL-85-110, vol. 2, p. 441 (1985).
2. P. A. Seeger, A. Williams and J. Trewhella, Proceedings of the Ninth Meeting of the International Collaboration on Advanced Neutron Sources, Villigen, Switzerland, Sept. 22–26, 1986.
3. P. A. Seeger and R. Pynn, *Nucl. Instr. and Meth.*, **A245** 115 (1986).
4. P. A. Seeger, *Nucl. Instr. and Meth.*, **178**, 157 (1980).
5. C. J. Glinka, J. M. Rowe and J. G. LaRock, *J. Appl. Cryst.* **19**, 427 (1986).
6. J. K. Kjems, R. Bauer, B. Breiting and A. Thuesen, in *Neutron Scattering in the 'Nineties*, (IAEA, Vienna, 1985), pp. 489–493.
7. P. A. Seeger, *IEEE Trans. Nucl. Sci.*, **NS-31**, 274 (1984).
8. "TUTSIM" is a registered trademark of APPLIED i, Palo Alto, CA (1986).
9. "MicroCAP II" is a registered trademark of Spectrum Software, Sunnyvale, CA (1986).
10. R. O. Nelson, D. M. Burrus, G. Cort, J. A. Goldstone, D. E. McMillan, R. V. Poore and D. R. Machen, *IEEE Trans. Nucl. Sci.*, **NS-32**, 1422 (1985).
11. R. V. Poore, D. M. Burrus, G. Cort, J. A. Goldstone, L. Miller and R. O. Nelson, *IEEE Trans. Nucl. Sci.*, **NS-32**, 1290 (1985).
12. R. P. Hjelm, *J. Appl. Cryst.*, **20**, 273 (1987).
13. R. P. Hjelm, *J. Appl. Cryst.*, **21**, 618 (1988).
14. G. D. Wignall and F. S. Bates, *J. Appl. Cryst.*, **20**, 28 (1987).
15. K. Ibel and A. Wright, ILL Internal Scientific Report 80IB45S (1980).